

Electronic structure and magnetic properties of the linear chain cuprates Sr_2CuO_3 and Ca_2CuO_3

H. Rosner, H. Eschrig, and R. Hayn

Max-Planck-Arbeitsgruppe 'Elektronensysteme', TU Dresden, D-01069 Dresden, Germany

S.-L. Drechsler* and J. Málek**

Institut für Festkörper- und Werkstofforschung Dresden e.V., Postfach 270016, D-01171 Dresden, Germany

(May 3, 2019)

Abstract

Sr_2CuO_3 and Ca_2CuO_3 are considered to be model systems of strongly anisotropic, spin-1/2 Heisenberg antiferromagnets. We report on the basis of a band-structure analysis within the local density approximation and on the basis of available experimental data a careful analysis of model parameters for extended Hubbard and Heisenberg models. Both insulating compounds show half-filled nearly one-dimensional antibonding bands within the LDA. That indicates the importance of strong on-site correlation effects. The bonding bands of Ca_2CuO_3 are shifted downwards by 0.7 eV compared with Sr_2CuO_3 , pointing to different Madelung fields and different on-site energies within the standard *pd*-model. Both compounds differ also significantly in the magnitude of the inter-chain dispersion along the crystallographical **a**-direction: ≈ 100 meV and 250 meV, respectively. Using the band-structure and experimental data we parameterize a one-band extended Hubbard model for both materials which can be further mapped onto an anisotropic Heisenberg model. From the inter-chain dispersion we estimate a corresponding inter-chain exchange constant $J_{\perp} \approx 0.8$ and 3.6 meV for Sr_2CuO_3 and Ca_2CuO_3 , respectively. Comparing several approaches to anisotropic Heisenberg problems, namely the random phase spin wave approximation and modern versions of coupled quantum spin chains approaches, we observe the advantage of the latter in the reproduction of reasonable values for the Néel temperature T_N and the magnetization m_0 at zero temperature. Our estimate of J_{\perp} gives the right order of magnitude and the correct tendency going from Sr_2CuO_3 to Ca_2CuO_3 . In a comparative study we also include CuGeO_3 .

71.15.Fv Atomic and molecular orbital methods

71.27.+a Strongly correlated electron systems

74.25.Jb Electronic structure

74.72.Jt other cuprates

75.30.Et Exchange and super-exchange

75.50.El Antiferromagnetics

Typeset using REVTeX

I. INTRODUCTION

Initiated by the discovery of high- T_c superconductivity in cuprate compounds, there is a renewed and growing interest in the electronic and magnetic properties of quasi one-dimensional (1D) structures near half band filling. Anionic quasi 1D CuO_3 chains of oxygen corner sharing CuO_4 plaquettes are present in Sr_2CuO_3 and in Ca_2CuO_3 [1,2], and CuO_2 chains of edge sharing plaquettes are present in CuGeO_3 [3]. Moreover, the first two of these compounds can be regarded as ‘parent’ compounds of more complex structures as the double chain compound SrCuO_2 (which, in notation $\text{Sr}_2\text{Cu}_2\text{O}_4$, is obtained from Sr_2CuO_3 by replacing the CuO_3 chain with a Cu_2O_4 double chain), and of a whole family of celebrated multi-leg ladder compounds $\text{Sr}_{2n}\text{Cu}_{2n+2}\text{O}_{4n+2}$ [4]. A detailed theoretical description of the ‘parent’ compounds is naturally a prerequisite for understanding all those materials. It is also desirable in view of the related two-dimensional (2D) cuprate structures of the high- T_c materials [5–11], and particularly in view of possible dynamical stripe superstructures in the latter [12].

Experimentally, Sr_2CuO_3 and Ca_2CuO_3 are found to be the best realizations of the quasi 1D spin-1/2 antiferromagnetic Heisenberg model (AHM). Their Néel temperatures, $T_N \approx 5\text{K}$ for Sr_2CuO_3 and $T_N \approx 9\text{K}$ for Ca_2CuO_3 , are very low compared to the intra-chain exchange integrals $J_{\parallel} \sim 0.2\text{ eV}$, and the ordered moments ($<0.1\ \mu_{\text{Bohr}}$) are extremely small [13–15]. The value $J_{\parallel} = 190\text{ meV}$ for Sr_2CuO_3 [10] appears to be the record value of an exchange integral among all known quasi 1D antiferromagnets. The correct description of the physics of a magnetic quasi 1D system with a weak magnetic inter-chain interaction has recently attracted much theoretical attention, see, e.g., Refs. [16–19]. For all these reasons, Sr_2CuO_3 has been announced to become a ‘superstar’ in the field of low-dimensional magnetism in near future [20].

In the work of Ami *et al.* [8], with the assumption of only a very weak dipolar inter-chain interaction constant $J_{\perp} \approx 0.01\text{ meV}$ and on the basis of RPA spin wave theory, for Sr_2CuO_3 a Néel temperature below 0.03K [21] was conjectured. At that time, due to resolution problems and because of the very small ordered moment $<0.1\mu_{\text{Bohr}}$, neutron diffraction on powders failed to detect antiferromagnetic ordering down to 1.5K . However, the relatively small inter-chain distances of 3.3 to 3.5\AA suggest that direct inter-chain hopping, which leads to a much stronger kinematic exchange interaction, cannot be neglected. The discussion of consequences for the magnetic properties forms a main issue of the present paper.

While numerous band-structure calculations [22] and tight-binding parameterizations of one- and multi-band Hubbard model Hamiltonians [23] for the quasi 2D cuprate structures can be found in the literature, we are aware of only two band-structure calculations for a quasi 1D cuprate structure, both for CuGeO_3 [24,25]. On the basis of a wealth of available experimental data for CuGeO_3 large efforts are currently directed to the parametrisation of phenomenological antiferromagnetic spin-1/2 Heisenberg models and exten-

sions including frustration in the next-nearest neighbor intra-chain exchange [26–29]. To our knowledge, no parameterization on the level of Hubbard-type models has been undertaken as yet, although estimates within the Anderson impurity model [30] were pointing to strong correlation. The understanding of CuO_3 chain substances is less developed, especially with respect to inter-chain interactions, and we shall present here a comparative analysis of both cases.

In contrast to the antiferromagnetic ordering of Sr_2CuO_3 , the less anisotropic compound CuGeO_3 exhibits a spin gap state below $T_{SP}=14.2\text{K}$ which is accompanied by the occurrence of a period-2 superstructure with a very small dimerization amplitude of $u_0 \approx 0.007\text{\AA}$. Therefore it has been interpreted as a spin-Peierls (SP) state. The SP state is supported by frustrated second neighbor exchange [26]. When doped with Zn for Cu or with Si for Ge, also a coexisting Néel state has been found below 4.5K [31,32]. The thereby observed magnetic moment, for example of $0.23\mu_{\text{Bohr}}$ in $\text{Cu}_{1-x}\text{Zn}_x\text{GeO}_3$, is significantly larger than the corresponding value of $0.06\mu_{\text{Bohr}}$ observed in Sr_2CuO_3 [13], suggesting a much larger anisotropy of the latter compound.

Within the frame of strongly anisotropic three-dimensional Heisenberg models, all considered compounds should be described by a dominating intra-chain exchange coupling, a small exchange coupling in direction of the shortest inter-chain spacing which reduces the strong quantum fluctuations and provides a non-zero ordered magnetic moment in the ground-state, and a generally very small inter-chain coupling in the third direction to ensure a non-zero Néel temperature in accord with the Mermin-Wagner theorem. By applying the results of available theoretical approaches to the anisotropic two- and three-dimensional Heisenberg models [16–18,33] one may extract phenomenological estimates of the exchange parameters for the chain cuprates, which then can be compared to results of electronic structure theory. Interestingly, different approaches yield significantly different predictions. The accurate determination of the Néel temperature of a strongly anisotropic Heisenberg magnet is still an unsolved and challenging theoretical task. We review here two frequently used approaches and compare their predictions from our estimates of exchange parameters with experimental data.

In the following Sec. II we present band-structure results for Sr_2CuO_3 and Ca_2CuO_3 which were obtained by applying a linear-combination-of-atomic-orbitals scheme to self-consistently solve the Kohn-Sham equation with the local-density approximation to the exchange and correlation potential (LDA-LCAO). This approach provides us in a most natural way with tight-binding parameters. Using these results and experimental estimates for short-range correlation effects, in Sec. III a single CuO_3 chain is represented by an extended Hubbard model and compared to the situation with CuGeO_3 . The magnitude of inter-chain exchange is estimated on this basis. In Sec. IV, estimates of Néel temperatures and ordered magnetic moments are derived by applying both standard RPA spin wave theory and modern quantum spin chain theory. The results are summarized in Sec. V, and an outlook is given.

II. BAND-STRUCTURE AND INTER-CHAIN TRANSFER

The crystal structure of the isostructural compounds Sr_2CuO_3 and Ca_2CuO_3 is depicted in Fig. 1. Chains of oxygen corner sharing CuO_4 plaquettes run along the **b**-direction. The in-chain Cu-O bond-length is 1.96 Å and practically the same in both compounds while the Cu-O bond-lengths in **c**-direction differ: 1.95 Å in Sr_2CuO_3 and 1.89 Å in Ca_2CuO_3 . The two inequivalent oxygen sites are referred to as chain oxygen and side oxygen in the following. The shortest inter-chain distance occurs in **a**-direction and differs substantially for both cases: 3.49 Å in Sr_2CuO_3 and 3.28 Å in Ca_2CuO_3 .

The self-consistent LDA-LCAO method has been applied to both compounds with a minimum basis treating the Cu-($4s, 4p, 3d$), O-($2s, 2p$), Sr-($5s, 5p, 4d$) and Ca-($4s, 4p, 3d$) orbitals as local valence basis states and the lower orbitals as core states. The crystal potential is calculated from overlapping spherical site densities. All basis states are calculated in the spherical site contribution to the crystal potential and recalculated in each iteration step. The valence basis orbitals have been compressed by an additional attractive potential to reduce the overlap among them [34]. Due to the relatively open crystal structure two empty spheres per unit cell have been introduced with empty sphere *s* and *p* orbitals at each site. For the exchange and correlation potential the parameterization of von Barth and Hedin was chosen and it has been calculated in atomic sphere approximation. We show in Fig. 2 the band-structure and in Fig. 3 the density of states (DOS) of Sr_2CuO_3 . The corresponding results for Ca_2CuO_3 are similar. The quantitative differences between both compounds are discussed below. To check the LCAO-band-structure by another method, we performed also calculations using the linear muffin-tin orbital (LMTO) approximation. We found no substantial differences, only the overall bandwidth of the whole *pd* band complex was found to be somewhat smaller in the LMTO results (see numbers below).

As expected from simple chemical considerations of covalency, there is a single, well separated, nearly one dimensional, half-filled antibonding band crossing the Fermi level with large dispersion in **b**-direction (see Fig. 2). The width of this band is about 2.2 eV (LCAO) or 2.0 eV (LMTO) for both compounds. The characteristic quasi-1D van Hove singularities near the band edges are clearly seen in the DOS (see Fig. 3). A tight-binding analysis of the orbitals involved shows that in first approximation the Cu $3d_{z^2-y^2}$ as well as the side oxygen $2p_z$ and the chain oxygen $2p_y$ orbitals are of direct relevance. Only a negligible admixture of Cu $4s$ states can be detected near both edges of this antibonding half-filled band. Its weight as determined by the ratio of the corresponding areas under the DOS curves (see insert of Fig. 3) is relatively small (0.3 per cent for Sr_2CuO_3), but it increases to a weight of 2 per cent for the Ca compound.

The metallic behaviour of the LDA band-structure is in sharp contrast to the experimental observation of large optical gaps ~ 2 eV which are comparable to the bandwidth obtained above. This points to the necessity of dealing

explicitly with the strong on-site Coulomb repulsion at the copper-site. The experimental gap cannot be explained by a spin density wave since it is large and persists also above the Néel temperature T_N . Instead we have to anticipate the situation of a charge transfer gap between valence states of mostly oxygen character and a copper upper Hubbard band above the Fermi level.

In analogy to cuprates with CuO_2 planes the construction of a multi-band, Hubbard-like model Hamiltonian would therefore be desirable. However, it is well known that such a Hamiltonian can be projected to an effective one-band picture which properly describes the low-energy physics [35,36]. The existence of a well isolated, one dimensional band in the present situation (shown in Fig. 4 in more detail) suggests such a possibility all the more. We assume that the parameters for the one band description can be determined by fitting the band of Fig. 4 to a dispersion of the form

$$\varepsilon(\vec{k}) = -2t_{1,LDA} \cos(k_y b) - 2t_{2,LDA} \cos(2k_y b) - 2t_{\perp} \cos k_x a \quad (1)$$

which yields the values listed in the Table [37].

In Fig. 4 the dispersion in the **a**-direction is clearly visible as an energy increase with increasing k_x by nearly the same amount both at the bottom and the top of the band. This dispersion is present through the band and gives a value of $t_{\perp} = 25$ meV. To be more accurate we determined t_{\perp} from the dispersion at the Fermi level which is shown in the insert of Fig. 4. The corresponding dispersion for Ca_2CuO_3 is significantly larger, by a factor of 2.5 (2.0 in LMTO). The smaller lattice constant of Ca_2CuO_3 leads to an increase of the inter-chain overlap of the Cu- d and O- p basis orbitals, but this effect alone is too small to explain the strong enhancement. We have checked that the transfer in **a**-direction goes dominantly via the cation Sr and Ca, respectively. The two-center Hamilton matrix elements between side oxygen and Ca are two times larger than the corresponding ones for Sr.

Dispersion in the **c**-direction is found within the level of accuracy of the band-structure calculations only (~ 5 meV). This practically missing dispersion in the **c**-direction indicates also that the inter-chain hopping in **a**-direction takes place horizontally only, with no zigzag contribution in (111) direction from side oxygen to side oxygen.

The comparison of the band structures of the Sr and the Ca compounds shows yet another interesting feature: namely, the bonding bands between -8.5 eV and -11.5 eV for Sr_2CuO_3 are shifted downwards by 0.6 to 0.7 eV for the Ca compound indicating a significantly different Madelung field. For the same reason the side oxygen in the Ca-compound comes out more negatively charged although the hybridization of its p_z -orbital with the Cu $3d_{z^2-y^2}$ orbital is slightly increased due to the shortened bond-length. This different on-site energies may have an influence on the different charge transfer energies as discussed in the next section.

We also analyzed in the same manner (Eq. 1) the linearized augmented plane waves (LAPW) energy bands for CuGeO_3 reported by Mattheiss [24]. CuGeO_3 differs from the chain cuprates considered above in the structure

of the chains. The CuO_2 chains of oxygen edge-sharing CuO_4 plaquettes of CuGeO_3 result in a more complex highest antibonding band in which two O- p states per oxygen site hybridize with the Cu- d orbital. The more complex composition of the crystal also manifests in the band-structure. In particular, due to the sizeable inter-chain interaction mediated by Ge and due to the presence of two chains per unit cell there are two differently filled split-off antibonding bands. For our qualitative comparison with the above considered chains (CuO_3 chain), we replace them by one half-filled band for the sake of simplicity. The tight-binding parameters of CuGeO_3 (Table) contain a significantly smaller nearest neighbor transfer integral $t_{1,LDA} \approx 0.25$ eV and an anomalously large next nearest neighbor integral [50] $t_{2,LDA} \approx 0.67t_1 = 0.18$ eV estimated from Fig. 2 of Ref. [24]. The large difference of the transfer integrals $t_{1,LDA}$ between chains of corner sharing plaquettes and CuGeO_3 should be related to the efficient 180° Cu-O-Cu hopping for the former (σ $p-d$ bond) compared with the inefficiency of non- σ $p-d$ hopping (nearly 135° (45°)) for CuGeO_3 ; for further details see Ref. [38]. This special structure explains also the relative large next nearest neighbor transfer integrals t_2 in CuGeO_3 due to the involved effective σ p_z - p_z hopping along the chain. The inter-chain hopping t_\perp can be deduced from the dispersion in the \mathbf{b} -direction of the LAPW energy bands of CuGeO_3 and is of the same order as in Sr_2CuO_3 and Ca_2CuO_3 .

Based on both the available experimental data and the band structure information obtained here, a semi-microscopic strong correlation model will be constructed which then can be mapped approximately onto a spin-1/2 Hamiltonian to describe the magnetic properties. This is the objective of the next section.

III. MICROSCOPIC DESCRIPTION IN TERMS OF THE EXTENDED HUBBARD AND ANISOTROPIC HEISENBERG MODELS

A. General relations

Here we parameterize the well-known extended Hubbard model for one single chain with hopping terms to first (t_1) and second neighbors (t_2):

$$\begin{aligned}
H = & - \sum_{m;j=1,2;s} t_j \left(c_{m,s}^\dagger c_{m+j,s} + h.c. \right) + \frac{U}{2} \sum_{m;s} c_{m,s}^\dagger c_{m,s} c_{m,-s}^\dagger c_{m,-s} \\
& + \sum_{m;j=1,2} V_j n_m n_{m+j} - |K| \sum_i \vec{S}_i \vec{S}_{i+1},
\end{aligned} \tag{2}$$

where $n_m = \sum_s c_{m,s}^\dagger c_{m,s}$ is the density operator and s denotes the spin index. We included in (2) a small, but non-negligible direct ferromagnetic exchange which naturally appears if we map a multi-band, Hubbard-like Hamiltonian to a one band model [35]. Its necessity and its main effects will be discussed below.

For the low-energy physics, at half-filling the extended Hubbard model (2) can be replaced to leading order in t/U by a spin-1/2 Heisenberg chain. It includes also a second neighbor exchange J_2 [39] and reads

$$H = J_1 \sum_i \vec{S}_i \vec{S}_{i+1} + J_2 \sum_i \vec{S}_i \vec{S}_{i+2},$$

$$J_1^{AF} = \frac{4t_1^2}{U - V_1}, \quad J_2 = \frac{4t_2^2}{U - V_2}, \quad (3)$$

where the effective exchange integral J_1 of the spin-1/2 Heisenberg Hamiltonian of cuprates is reduced from the predominant antiferromagnetic superexchange part by the ferromagnetic contribution (2)

$$J_1 \approx -|K| + J_1^{AF}. \quad (4)$$

Notice that within this approach J_2 yields a competition (frustrated) character to the usually dominant short range antiferromagnetic correlations which are established by J_1 . That term is especially important for CuGeO_3 .

The two main parameters U and t_1 of the effective extended Hubbard model are directly related to the optical gap E_g and the exchange integral between nearest neighbors J_1 which are experimentally accessible. The following analysis is considerably simplified if the materials of interest are in the strongly correlated limit $U > 4t$ and excitonic effects at zero momentum transfer q are not very strong i.e. $U \gg t_j > V_j$; $j = 1, 2$. The parameter sets derived below support such a point of view. We take into account the effect of the intersite Coulomb interaction V_1 by renormalizing the on-site correlation in the form $U_{eff} = U - V_1$. Then we may use the optical gap E_g obtained from the Bethe-Ansatz solution for the pure 1D Hubbard model given by Ovchinnikov [40],

$$E_g = \frac{16t_1^2}{U_{eff}} \int_1^\infty \frac{\sqrt{x^2 - 1} dx}{\sinh(2\pi t_1 x / U_{eff})}$$

$$\approx U_{eff} - 4t_1 + 2\ln 2 J_1^{AF} \quad \text{for } U_{eff} \gg t_1; \quad J_1^{AF} = 4t_1^2 / U_{eff}. \quad (5)$$

In the strong coupling case Eq. (5) can be transformed to the useful relation

$$t_1 = 0.5 J_1^{AF} \left(1 + \sqrt{E_g / J_1^{AF} + 1 - 2\ln 2} \right). \quad (6)$$

It has been assumed that the smaller parameters t_2 and $|K|$, i.e. the hopping to second neighbors and the ferromagnetic exchange in (2), have no substantial influence on the charge transfer gap (but t_2 enhances the spin gap in the spin-Peierls state).

The presence of a weak second neighbor exchange can be approximately described in some cases by an effective renormalized nearest neighbor exchange integral [44,45]

$$J = J_1 - rJ_2 \approx J_1 - J_2, \quad (7)$$

where $r = 1$ according to Ref. [44] and $r = 1.12$ according to Ref. [45]. Recently, Stephan and Penc [46] predicted a strong narrow excitonic peak in the density-density response function $N(q, \omega)$ of the EHM in the strong coupling limit at the zone boundary $q = \pi/b$:

$$\omega_{ex}(\pi/b) = U - V_1, \quad (8)$$

provided $V_1 > 0$.

B. Parameter assignment

In principle, we can determine U_{eff} and t_1 from the experimentally measured E_g and J values using Eqs. (4–7) which are presented graphically in Fig. 5. In the case of Sr_2CuO_3 , very recently also the narrow excitonic peak at the zone-boundary (8) and with it U_{eff} were determined experimentally [49].

However, to the best of our knowledge, the available experimental information on all three systems is incomplete or contradicting each other. For instance, for Ca_2CuO_3 the charge gap determined from the maximum of $\Im m \varepsilon(\omega)$ is $E_g = 2.1$ eV [5], but a direct measurement of the J value from the magnetic susceptibility does not exist. Interpreting the midinfrared absorption as a phonon-assisted two magnon process a value of $J = 255$ meV was reported [47]. For Sr_2CuO_3 the experimental J values range from 140 to 260 meV [9,10,47]. In the following we shall use 190 meV as a representative value. According to quite recent data for this system the one-dimensional charge transfer gap $E_g(\text{Sr}) \approx 1.9 \pm 0.1$ [49] might be somewhat smaller as compared to the Ca compound. Strictly speaking, the optical absorption sets in already near 1.5 eV [41,42,49]. The elucidation of the observed broadening of the expected 1D van-Hove singularity in terms of the inter-chain interaction, quantum fluctuations, disorder, and/or excitonic and other many-body effects is a difficult problem beyond the scope of the present paper.

Taking this situation into account, we use the available experimental data and also our band-structure results to derive a consistent parameter set of (2) (t_1, t_2, U_{eff}, V_1 and $|K|$) for each of the three substances, separately. Vice versa, the demand of internal consistency weights the experimental information.

1. Sr_2CuO_3

Recent electron energy loss spectroscopy data of Neudert *et al.* [49] allow to determine $U_{eff} = 3.15 \pm 0.1$ eV from the maximum of $\Im m \varepsilon(\omega)$ at the zone boundary (8). At the same time E_g was measured to be 1.9 ± 0.1 eV from the data at small momentum. Similarly $E_g = 1.92$ eV was found from the

Raman resonance energy [11] observed for diagonal in-chain (yy) polarization only. Our aim is to derive values for the magnetic coupling constants from Eqs. (4-7) with the use of experimental values of U_{eff} and E_g . Since it turns out that the derived J -values depend sensitively on U_{eff} and E_g , we consider two sort of extreme cases. From Eq. (5) we obtain $t_1 = 0.410\text{eV}$ with $U_{eff} = 3.15\text{ eV}$ and $E_g = 1.8\text{ eV}$ (lower bound). That corresponds to $J_1^{AF} = 213\text{ meV}$. According to Eqs. (4,7) that value has to be reduced by the frustrated next nearest neighbor exchange J_2 of about 12 meV (corresponding to $t_2 = 100\text{ meV}$ from our tight binding fit) and by the ferromagnetic contribution $|K|$ before it can be compared with the total experimental exchange integral $J = 190 \pm 17\text{ meV}$ [10]. Thus we can estimate a direct ferromagnetic exchange of $|K| \approx 11 \pm 17\text{ meV}$. The slightly smaller K value compared with 35 meV for La_2CuO_4 obtained in Ref. [35] might be attributed to the shorter Cu-O bond-length of 1.89 Å for the latter compound. The so derived parameter set is listed in the Table. We derived a second parameter set with a considerable smaller value of J_1 by taking $E_g = 1.95\text{ eV}$ and $U_{eff} = 3.25\text{ eV}$ near the upper bounds of the experimental results. We obtain from (5) $t_1 = 0.394\text{ eV}$ and correspondingly $J_1^{AF} = 190\text{ meV}$. Such a parameterization is compatible with the total exchange integral $147_{-9}^{+13}\text{ meV}$ [9] derived from the magnetic susceptibility data. We note that both parameterizations are incompatible with the large J values of 246 meV [48] and 261 meV [47] derived from midinfrared optical absorption data (the small differences between the latter values arise mainly from the adopted phonon frequency of 70 and 80 meV, respectively, involved in the phonon-assisted absorption process) provided there is no sizeable *ferromagnetic* second neighbor exchange overcompensating the ferromagnetic nearest neighbor contribution $|K|$ and the antiferromagnetic next nearest neighbor superexchange $J_2 = 4t_2^2/U_{eff}$. Anyhow, the elucidation of the microscopic origin of the apparent discrepancy between the magnetic susceptibility and the midinfrared optical absorption data analyzed in terms of the simple nearest neighbor spin-1/2 Heisenberg model remains a challenging problem.

2. Ca_2CuO_3

The slightly larger charge transfer gap of 2.1 eV suggests also an enhanced U_{eff} -value in comparison with the Sr-compound. That means that it is again difficult to find a reasonable parameterization which is compatible with the large J value of 254 meV from midinfrared absorption data. Due to the lack of experimental information on the magnetic susceptibility we use in the following our theoretical estimate of 160 meV for the J value of Ca_2CuO_3 [36]. Adding a ferromagnetic contribution of $|K| \approx 30\text{ meV}$ (of the same order as for La_2CuO_4) and a frustrating $J_2 \approx 10\text{ meV}$ we may find $J_1^{AF} = 200\text{ meV}$. Of course, in the given case this should be considered as a very rough estimate. Then, together with $E_g = 2.1\text{ eV}$, we calculate from (6) $t_1 = 418\text{ meV}$. According to (5) that corresponds to $U_{eff} = 3.5\text{ eV}$, showing the expected

enhancement. On the level of the pd -model the reason for the enhanced effective on-site interaction should be traced back to a larger $\Delta\varepsilon_{pd} \approx U_{eff}$. It seems to be related to a Madelung effect caused by the difference in the lattice parameters of the Sr and Ca compound, respectively. This point of view is corroborated by our band-structure calculations discussed in the previous section: for Ca_2CuO_3 the distance between the half-filled antibonding band and the filled bonding bands is larger by 0.7 eV compared to the Sr case.

3. Inter-site Coulomb repulsion and comparison with CuGeO_3

According to the microscopic calculations of Geertsma and Khomski [38] the total nearest neighbor exchange integral of CuGeO_3 $J_1(\text{Ge})=11.6$ meV can be decomposed into an antiferromagnetic contribution of $J_1^{AF} = 30.4$ meV and into a relatively large ferromagnetic one of $|K| = 18.8$ meV. Let us stress again that the effective nearest neighbor transfer integral t_1 and the on-site interaction U_{eff} are directly related to the antiferromagnetic part only. For CuGeO_3 charge transfer gaps of 3.66 eV [30] and 1.25 eV [43] have been reported [50]. Using $E_g = 3.7$ eV and $J_1^{AF} = 30.4$ meV, the main parameters of the extended Hubbard model come out as $t_1 = 0.187$ eV and $U_{eff} = 4.34$ eV. Interestingly, the latter value nearly perfectly coincides with the charge transfer energy $\Delta=4.2$ eV found out from the XPS data analyzed within the Anderson impurity model in Ref. [30]. Within a pd -model the significantly enhanced corresponding $\Delta\varepsilon_{pd}$ value should be attributed to the Ge-cations located near the CuO_2 chain oxygens. This point of view is supported by the following observations. In compounds like $\text{Sr}_{14}\text{Cu}_{24}\text{O}_{41}$ where the CuO_2 chains under considerations are surrounded by earth alkaline cations the corresponding charge gap is reduced to about 2.8 eV [51]. For that compound, $\Delta\varepsilon_{pd}$ as calculated within the ionic point charge model amounts to 3.7eV [52].

Comparing the data collected in the Table we suggest that Ca_2CuO_3 should be somewhat stronger correlated than its Sr counterpart. Without doubt, the most strongly correlated compound among them all is CuGeO_3 having the smallest transfer integral $t_1(\text{Ge})=0.187$ eV and the largest $U_{eff}(\text{Ge}) = 4.34$ eV. The large ratios U_{eff}/t_1 obtained in all three cases (7.7(Sr), 8.4(Ca), and 23(Ge)) justify *a posteriori* the use of Eq. (5).

The difference between t_1 and $t_{1,LDA}$ may be explained by a renormalization of the transfer integral t_1 by the inter-site Coulomb interaction V_1 . Within the Hartree-Fock approximation, the correction due to V_1 leads to a renormalized effective hopping integral $t_1 + pV_1$ with the bond order $p \sim 2/\pi$. This renormalized hopping integral can be compared with $t_{1,LDA}$ where the inter-site Coulomb interaction is already partially taken into account. From $t_{1,LDA} = t_1 + pV_1$ and the data of t_1 and $t_{1,LDA}$ given in the Table we may determine $V_1 = 0.21$ eV for Sr_2CuO_3 , $V_1 = 0.16$ eV for Ca_2CuO_3 , and $V_1=0.1$ eV for CuGeO_3 (here $t_1 = 0.187$ eV as estimated above has been adopted). Thus, the inter-site Coulomb interactions $V_1 \lesssim 0.2$ eV of all three compounds

are quite close to each other and fulfill the relation $V_1 \ll U$. Notice that these numbers for V_1 roughly agree with the corresponding 2D-values 0.11 eV or 0.17 eV given in Refs. [35,53], respectively, and the estimate based on the four-band model for CuO_3 chains [54]: $V_1 \approx n_d n_p V_{pd} + n_d^2 (V_{dd} - V_{2,dd}) \approx 0.23$ eV, where typical occupation numbers $n_d \approx 0.7$, $n_p \approx 0.13$ and $V_{pd} = 1.2$ eV for the copper oxygen inter-site Coulomb interaction and $V_{1,dd} = 0.5$ ($V_{2,dd} = 0.25$) eV for the (next) nearest neighbor copper copper inter-site Coulomb interaction have been taken.

The value for t_2 in the Table was either taken from the fit to the band-structure data ($= t_{2,LDA}$ for Sr_2CuO_3 and Ca_2CuO_3) or inferred from the experimentally known value for $J_2 = 4.3$ meV [26] for CuGeO_3 using Eqs. (5).

4. Inter-chain exchange

Now, we would like to give a first estimate of the magnetic couplings between chains. The inter-chain exchange interaction J_\perp in the \mathbf{a} -direction for Sr_2CuO_3 and Ca_2CuO_3 (corresponding to the \mathbf{b} -direction in CuGeO_3) will be approximated by

$$J_\perp = \frac{4t_\perp^2}{U_{eff}}, \quad (9)$$

where we assumed for simplicity the same inter-site Coulomb interaction V_1 within the chain and perpendicular to it. The corresponding values are listed in the Table. The discussion above about a possible direct ferromagnetic exchange which leads to a systematic reduction of exchange integrals suggests that these values should be considered as upper bounds. In the case of CuGeO_3 the so determined $J_\perp = 1$ meV can be compared with experimental data from neutron scattering [55,27] $J_\perp \approx 1.1$ meV showing a reasonable agreement. Notice that in the case of Sr_2CuO_3 our inter-chain interaction exceeds the dipolar interaction evaluated in Ref. [8] by two orders of magnitude.

The magnitude of the weakest interaction $J_{\perp,c}$ in the \mathbf{c} -direction is difficult to estimate theoretically for several reasons. It was already discussed that a band-structure hopping integral cannot be given at present. In any case it may be expected that $J_{\perp,c}$ is smaller than the other exchange integrals by several orders of magnitude and is difficult to calculate in any case. Treating $J_{\perp,c}$ therefore as a purely phenomenological parameter in the following, we will use to be specific (if necessary) the same value for Ca_2CuO_3 as has been evaluated in Ref. [8] for Sr_2CuO_3 , adopting the dipolar interaction for $J_{\perp,c} \approx 10^{-4}$ meV.

IV. SOME ASPECTS OF THE NÉEL STATE

The magnetic properties of undoped cuprates (i.e. one hole per Cu site in the standard pd -model) are usually described by the anisotropic spin-1/2 antiferromagnetic Heisenberg model

$$H = \sum_{\langle i,j \rangle} J_{ij} \mathbf{S}_i \mathbf{S}_j \quad , \quad (10)$$

with $J_{ij} = J_{\parallel} (= J_1)$ for (ij) being nearest neighbors in the chain direction (that is the \mathbf{b} -direction for Sr_2CuO_3 and Ca_2CuO_3) and J_{\perp} for nearest neighbor copper sites in \mathbf{a} -direction (see Fig. 1). The weakest interaction will be denoted here by $J_{\perp,c}$. According to the results of the previous sections and from the experimental data we know that Sr_2CuO_3 and Ca_2CuO_3 are characterized by very anisotropic interaction strengths

$$J_{\parallel} \gg J_{\perp} \gg |J_{\perp,c}|, \quad (11)$$

the anisotropy being about three orders of magnitude for each inequality. Instead of the spin-Peierls system CuGeO_3 , in this section for comparison we will consider the doped compound $\text{GeCu}_{1-x}\text{Zn}_x\text{O}_3$ ($x=0.034$) [31,32] which shows antiferromagnetic order. This is an example for an anisotropic Heisenberg problem with weaker anisotropy than Sr_2CuO_3 and Ca_2CuO_3 . For simplicity, we will use for $\text{GeCu}_{1-x}\text{Zn}_x\text{O}_3$ the same parameters which were derived in the previous section for CuGeO_3 . We also neglect here the frustrated exchange J_2 .

In the following we review several approaches for such anisotropic systems where quantum and thermal fluctuations become important. We will mention the usual spin wave approach in self-consistent random phase approximation (RPA-SWA) where all directions are treated on an equal and simple footing, and the coupled quantum spin chain approach (CQSCA) which involves a sophisticated treatment of the intra-chain direction and a mean-field treatment of the remaining perpendicular inter-chain interactions.

A. RPA spin wave theory

The RPA-SWA yields simple analytical expressions for the Néel temperature T_N and for the magnetization $\langle S_A^z \rangle = m_0$ at zero temperature (see [8], [56] and references therein). Both quantities can be derived from the expression

$$2m(T) = \frac{1}{1 + 2\psi}, \quad \psi = \frac{1}{N} \sum_{\vec{q}} \left(\frac{\omega_0}{\Omega(q)} \coth \left(\frac{\Omega(q)}{2T} \right) - 1 \right), \quad (12)$$

where

$$\Omega(q) = \sqrt{\omega_0^2 - \omega_1^2(q)}, \quad \omega_1 = 4m(T)J_{\parallel} (\cos q_y + R \cos q_x + R_c \cos q_z), \quad (13)$$

with $\omega_0 = 4m(T) (J_{\parallel} + J_{\perp} + J_{\perp,c})$, $R = J_{\perp}/J_{\parallel}$ and $R_c = J_{\perp,c}/J_{\parallel}$. We put $k_B = 1$. The Néel temperature is defined by the condition of vanishing magnetization which yields

$$2T_N = J_{\parallel}/I(R, R_c), \quad (14)$$

where

$$I(R, R_c) = \frac{1}{\pi^3} \int \int \int_0^\pi \frac{dq_x dq_y dq_z}{R(1 - \cos q_x) + R_c(1 - \cos q_z) + (1 - \cos q_y)}. \quad (15)$$

Expanding $I(R, R_c)$ for $J_\parallel \gg J_\perp \gg J_{\perp,c}$ gives the approximate expression

$$I(R, R_c) = \frac{0.66}{\sqrt{R}} (1 + 0.24(\ln(R/R_c) - R)), \quad (16)$$

which determines the Néel temperature together with (14). The zero temperature magnetization m_0 is in the same limit given by

$$m_0 = \frac{0.303}{1 - 0.386 \ln(R)}, \quad (17)$$

where the small parameter R_c turned out to be irrelevant. Notice that the RPA-description adopted reveals a vanishing magnetic moment in the $R \rightarrow 0$ limit. Thus it differs from the ordinary spin-wave theory which yields a diverging expression $m_0 = |0.5 + (1/\pi) \ln R|$ in the weak inter-chain coupling limit.

Let us now check the above expressions using the estimates of the last section and compare them with the experimental data. These data for T_N and the magnetic moment $\mu^{exp} = g_L m_0$ are given in the Table. In the following we will adopt a typical cuprate Landé factor $g_L \approx 2.1$ for Cu^{+2} [8]. Using the values J_\parallel and J_\perp from the Table and $J_{\perp,c} = 10^{-4}$ meV, we find $T_N^{Sr} = 38$ K, $T_N^{Ca} = 75$ K, $\mu^{Sr} = 0.20\mu_B$ and $\mu^{Ca} = 0.26\mu_B$ for the Sr and Ca compound, respectively. The ratio of the two experimental Néel temperatures agrees approximately with the RPA-SWA prediction

$$T_N^{Ca}/T_N^{Sr} \approx \sqrt{J_\parallel^{Ca} J_\perp^{Ca}} / \sqrt{J_\parallel^{Sr} J_\perp^{Sr}} \approx 2 \quad (18)$$

where the logarithmic corrections in Eq. (13) can be neglected since they are not very important for the above ratio. However, the absolute values of T_N within the RPA-SWA disagree with the experimental data. In the case of the more isotropic $\text{GeCu}_{1-x}\text{Zn}_x\text{O}_3$ we find $\mu^{Ge} = 0.32\mu_B$, i.e. a better agreement. But also here, the magnetic moment is overestimated by the RPA-SWA. In this case that may be ascribed to the effect of the frustrated second neighbor exchange.

For the Sr and Ca compounds one could try the opposite procedure using the given experimental data (including J_\parallel) to determine an “empirical” J_\perp^{emp} . Then one finds values for J_\perp^{emp} which are two (from T_N) or more than four (from m_0) orders of magnitude lower than those estimated in the previous section. This seems, therefore, to be unrealistic. Despite the fact that it gives the correct limits for m_0 both for $R \rightarrow 0$ and in the 2D isotropic case for $R \rightarrow 1$, the RPA-SWA seems to overestimate m_0 for large anisotropy ($R \ll 1$) quite considerably. That points to the necessity for an improved method. In the case of smaller anisotropy (e.g. $R \sim 0.1$ like for $\text{GeCu}_{1-x}\text{Zn}_x\text{O}_3$), the RPA-SWA seems to give more reliable results.

B. Coupled quantum spin chain approach (CQSCA)

Adopting Schultz's interchain RPA-expression (Eq. (7) of Ref. [16]), we replace $J_{\perp} \rightarrow 0.5(J_{\perp} + J_{\perp,c})$ as would be suggested by our strongly "orthorhombic" parameter regime $J_{\parallel} \gg J_{\perp} \gg J_{\perp,c}$. Then one arrives at

$$m_0 = \gamma\sqrt{R}, \quad (19)$$

where the proportionality factor γ is 0.72. (A similar factor $2/\pi=0.637$, was obtained by Fukuyama *et al.* [57]). The corresponding values for $\mu^{CSC} = g_L m_0$ are listed in the Table.

Analogously, within these theories one expects $T_N \approx J_{\perp}$ [17], in particular, the slightly modified implicit expression for the transition temperature proposed by Schulz [16] reads

$$T_N = \frac{2}{\pi} J_{\perp} \ln^{1/2} \left(\Lambda J_{\parallel} / T_N \right), \quad (20)$$

where $\Lambda \approx 5.8$.

From a principal point of view (Mermin-Wagner theorem), it is clear that Eq. (20) overestimates T_N because it does not depend on $J_{\perp,c}$. However, if one assumes that its influence can be described by logarithmic terms like in Eq. (16) which then ensure a finite T_N , the relative changes might be quite small.

Like in the RPA-SWA, our estimated values for J_{\perp} and the experimental J_{\parallel} lead to too large values for T_N and m_0 . But now, using the experimental m_0 and J_{\parallel} we can determine from Eq. (16) an "empirical" J_{\perp}^{emp} of the CuO_3 chain compounds which is of a similar order of magnitude to our estimates. The value of J_{\perp}^{emp} is smaller by a factor between 2 and 3 (Sr_2CuO_3 , $\text{GeCu}_{1-x}\text{Zn}_x\text{O}_3$), or 6 (Ca_2CuO_3) compared to the theoretically estimated values (see Table). The Néel temperature can also be used to determine J_{\perp}^{emp} which gives similar values showing the internal consistency of the CQSCA. But one should keep in mind that Eq. (18) does not fulfill the Mermin-Wagner theorem. In that respect we note here an alternative approach to the strongly anisotropic Heisenberg model (Castro Neto and Hohn [33]) in which the Néel temperature was found to depend linearly on $J_{\perp,c}$. Naturally, the elucidation of the correct description as to how this smallest interaction parameter does affect the finite temperature properties remains a challenging problem. Without its generally accepted solution it makes no sense to discuss the absolute values of the Néel-temperature beyond an order of magnitude accuracy.

One possible explanation for the reduction of J_{\perp}^{emp} in comparison with our estimated J_{\perp} could be the proximity of a spin-Peierls state. Phase fluctuation effects beyond the mean-field inter-chain approach used in deriving Eq. (19) can then become quite important. Following the renormalization group approach of Wang [19] for a plane of weakly interacting chains at $T = 0$, one finds a strongly renormalized magnetization which can be traced back to a renormalized exchange integral. If that is true, one should expect Ca_2CuO_3

to be much closer to the SP phase transition point than Sr_2CuO_3 . Furthermore for small exchange integrals compared with the phonon frequency (~ 10 to 20 meV), phonon exchange gives rise to a quasi-instantaneous interaction between localized spins, leading to a renormalization $J \rightarrow J_{eff} < J$ [59].

Another possible origin for the difference between J_{\perp} and J_{\perp}^{emp} might be our simple procedure to estimate J_{\perp} based on the extended Hubbard model. It was already mentioned that such a procedure has the tendency to overestimate the exchange integrals which becomes already apparent for J_{\parallel} . Last not least, one should keep in mind an uncertainty of the band-structure methods with respect to transfer integrals as small as in the considered case. The replacement of the full potential in the region in between the chains by empty spheres as explained in Sec. II might effect the transverse tails of the Wannier-functions which determine the value of the transfer integral t_{\perp} . A similar effect is expected if the exchange and correlational potential is supplemented with gradient terms reflecting the strong change in the electron density moving from one chain to its neighbors. Anyhow, one would expect roughly the same accuracy for the Sr and the Ca compound. In this context the much stronger deviation of the magnetic moment of the Ca compound might be related to somewhat reduced accuracy of Eq. (16) in less anisotropic cases.

V. SUMMARY

Band-structure calculations for Sr_2CuO_3 and Ca_2CuO_3 show in addition to the expected large dispersion along the chain direction also a remarkable dispersion in the crystallographic \mathbf{a} -direction, i.e. perpendicular to the plane containing the corner-shared CuO_4 plaquettes which form the CuO_3 chains. The corresponding inter-chain transfer gives rise to antiferromagnetic exchange integrals J_{\perp} in the meV range. Together with a small dipolar exchange in the third direction $J_{\perp,c}$ it explains the antiferromagnetic order in terms of an anisotropic Heisenberg model. The larger value of J_{\perp} for Ca_2CuO_3 corresponds with the larger Néel temperature and the larger magnetic moment [15] in comparison with Sr_2CuO_3 . However, our rough estimation of exchange integrals, based on the one band assumption, seems to overestimate the difference between both substances. CuGeO_3 is different from these two substances by a much smaller exchange in chain direction and a comparable large frustration parameter which suppresses the antiferromagnetic state and stabilizes the spin Peierls state. The smaller anisotropy becomes apparent in $\text{GeCu}_{1-x}\text{Zn}_x\text{O}_3$ where a Néel state was found with significantly larger magnetic moments than in Sr_2CuO_3 or Ca_2CuO_3 .

The copper oxygen chains of the three compounds under consideration can be described within an extended Hubbard model supplemented by ferromagnetic contributions to the nearest neighbor exchange integral. For the Ca and Sr compounds excitonic effects in the limit $q \rightarrow 0$ are expected to be weak due to small inter-site Coulomb interaction V_1 . But near the zone boundary $q \approx \pi/b$ strong excitonic effects are expected in the framework of the theory

developed recently by Stefan and Penc [46]. If our proposed parameterization is correct, for Ca_2CuO_3 (≈ 3.5 eV) and CuGeO_3 (≈ 4.3 eV) these excitonic peaks should be observed at higher energies than for Sr_2CuO_3 (3.15 eV).

The LDA band structure calculations yield useful insights into important material dependent parameters as inter-chain electron transfer and tendencies of the crystal field (Madelung) potential, varying from one substance to the other, albeit that the estimate of the on-site and inter-site Coulomb interaction requires more sophisticated methods such as LDA-calculations with local constraint.

According to our findings, Ca_2CuO_3 is expected to be a typical 1D charge transfer insulator analogously to the 2D model system $\text{Sr}_2\text{CuO}_2\text{Cl}_2$ although the inter-chain interaction is intermediate between the strongly correlated CuGeO_3 and the most 1D Sr_2CuO_3 . Possibly, the latter system is the weakest correlated one of the three. The compounds Sr_2CuO_3 and Ca_2CuO_3 offer also the opportunity to study in detail the effect of the inter-chain interaction provided it can be changed in a controlled way. Indeed, the study of the magnetic properties of the alloy system $\text{Sr}_{2-x}\text{Ca}_x\text{CuO}_3$ gives an interesting possibility to change continuously the magnitude of the inter-chain coupling. This is also interesting from the theoretical point of view since it gives a possibility to check in more detail sophisticated theories for weakly coupled quantum spin chains.

ACKNOWLEDGMENTS

Discussions with Profs. J. Fink, P. Fulde, D. Hone, H. Schulz, D. Johnston, and T. Van Oosten are acknowledged. Special thanks to Dr. M. S. Golden for discussions and a critical reading of the manuscript and to R. Neudert providing us with EELS data for Sr_2CuO_3 prior to publication. One of us (J. M.) thanks the Max-Planck-Institut “Komplexe Systeme” Dresden, for hospitality during which part of the present work was performed. Finally, the Deutsche Forschungsgemeinschaft is also acknowledged for financial support (S.-L. D. and J. M.) .

REFERENCES

- * Author to whom all correspondence should be addressed, email-address: drechsler@ifw-dresden.d400.de
- ** On leave from: Institute of Physics, Prague, Czech Republic.
- 1 C.L. Teske and H. Müller-Buschbaum, *Z. Anorg. Allg. Chem.* **371**, 325 (1969).
- 2 M. Hjorth and J. Hyldtoft, *Acta Chem. Scand.* bf 44, 516 (1990).
- 3 M. Hase, I. Terasaki, and K. Uchinokura, *Phys. Rev. Lett.* **70**, 3651 (1993).
- 4 K. Ishida, Y. Kitaoka, Y. Tokunga, S. Matsumoto, K. Asayama, M. Azuma, Z. Hiroi, and M. Takano, *Phys. Rev. B* **53**, 2827 (1996).
- 5 Slet Y. Tokura, S. Koshihara, T. Arima, H. Takagi, S. Ishibashi, T. Ido, and S. Uchida, *Phys. Rev. B* **41**, 11 657 (1990).
- 6 M. Yoshida, S. Tajima, N. Kozhizusuka, S. Tanaka, S. Uchida, and S. Ishibashi, *Phys. Rev. B* **44**, 11 997 (1991).
- 7 A. Keren, L.P. Le, G.M. Luke, B.J. Sternlieb, W.D. Wu, Y.J. Uemura, S. Tajima, and S. Uchida, *Phys. Rev. B* **48**, 12 926 (1993).
- 8 T. Ami, M.K. Crawford, R.L. Harlow, Z.R. Wang, D.C. Johnston, Q. Huang, and R. Erwin, *Phys. Rev. B* **51**, (1995).
- 9 S. Eggert, *Phys. Rev. B* **53**, 5116 (1996).
- 10 N. Motoyama, H. Eisaki, and S. Uchida, *Phys. Rev. Lett.* **76**, 3212 (1996); M. Takigawa, N. Motoyama, H. Eisaki, and S. Uchida, *Phys. Rev. Lett.* **76**, 4612 (1996);
- 11 O. Misochko, S. Tajima, C. Urano, H. Eisaki, and S. Uchida, *Phys. Rev. B* **53**, R14 733 (1996).
- 12 V. Emery, S. Kivelson, and O. Zachar, sissa-preprint cond-mat/9610094 (1996).
- 13 K. Kojima, M. Larkin, B. Nachumi, Y. Uemura, H. Eisaki, M. Motoyama, S. Uchida, B. Sternlieb, and G. Shirane, *Czechoslovak Journal of Phys.* **46**, Suppl. S4, 1945 (1996).
- 14 K. Yamada, J. Wada, S. Hosoya, Y. Endoh, S. Noguchi,
- 15 K. Kojima, Y. Fudamoto, M. Larkin, G. Luke, J. Merrin, B. Nachumi, Y. Uemura, N. Motoyama, H. Eisaki, S. Uchida, K. Yamada, Y. Endoh, S. Hosoya, B. Sternlieb, and G. Shirane, *Phys. Rev. Lett.* **78**, 1787 (1997).
- 16 H.J. Schulz, *Phys. Rev. Lett.* **77**, 2790 (1996).
- 17 I. Affleck, M. Gelfand, and R. Singh, *J. Phys. A* **27**, 7313 (1994), Erratum 28, 1787 (1995), and sissa-preprint cond-mat/9408062 (1994).
- 18 I. Affleck, and B. Halperin, sissa-preprint cond-mat/9603078 (1996).
- 19 Z. Wang, *Phys. Rev. Lett.* **78**, 126 (1997), cond-mat/9611129 (1996).
- 20 A. Tsvetik “Quantum Field Theory in Condensed Matter”, Cambridge University Press, p. 264, 155 (1995).
- 21 Adopting the applicability of the RPA-spin wave theory and the value of the weak dipolar interchain interaction of about 0.01 meV evaluated in [8] one would arrive at $T_N = 6.2$ K, i.e. accidentally close to the experimental value, in sharp contrast to the stated $T_N \approx 0.028$ K, only. Using the more realistic interchain value of about 1 meV obtained below, one arrives formally at $T_N \approx 29$ K. For a critical discussion of that approach see Sec. IV.
- 22 W. E. Pickett, *Rev. Mod. Phys.* **61**, 433 (1989).
- 23 M. S. Hybertsen, E. B. Stechel, M. Schlüter, and D. R. Jennison, *Phys. Rev. B* **41**, 11068 (1990).
- 24 L.F. Mattheiss, *Phys. Rev. B* **49**, 14 050 (1994).
- 25 Z. Popović, F. Vukajlović, and Z. Slivancanin, *J. Phys. Condens. Mat.* **7**, 4549 (1995).

- 26 J. Riera and A. Dobry, Phys. Rev. B **51**, 16 098 (1995).
- 27 L.P. Regnault, M. Ain, B. Hennion, G. Dhalenne, and A. Revcolevschi, Phys. Rev. B **53**, 5579 (1996).
- 28 H. Kuroe, J. Sasaki, T. Sekine, N. Koide, Y. Sasago, K. Uchinokura, and M. Hase, *sisso.cond-mat/9610134* and Phys. Rev. B, **55**, (1997), in press.
- 29 V. Muthukumar, C. Gros, W. Wenzel, R. Valentí, P. Lemmens, B. Eisener, G. Güntherodt, M. Weiden, C. Geipel, and F. Steglich, Phys. Rev. B **54**,R9635 (1996); V. Muthukumar, C. Gros, R. Valentí, M. Weiden, C. Geipel, F. Steglich, P. Lemmens, M. Fischer, and G. Güntherodt, *sisso-prep. cond-mat/9611018*.
- 30 F. Parmigiani, L. Sangaletti, A. Goldoni, U. del Pennino, C. Kim, Z.-X. Shen, A. Revcolevschi, and G. Dhalenne, Phys. Rev. B, **55**, 1459 (1997).
- 31 M. Hase, K. Uchinokura, R. Birgeneau, K. Hirota, and G. Shirane, J. Phys. Soc. Jap. **65**, 1392 (1996).
- 32 M. Poirier, R. Beaudry, M. Castonguay, M. Plumer, G. Quirion, F. Razavi, A. Revcolevschi, and G. Dhalenne, Phys. Rev. B **52**, R6971 (1995).
- 33 A.H. Castro Neto and D. Hone, Phys. Rev. Lett. **76**, 2165 (1996), D. Hone and A. Castro Neto, J. of Superconductivity **10** in press.
- 34 H. Eschrig, Optimized LCAO Method (Springer-Verlag, Berlin, 1989).
- 35 H.-B. Schüttler and A.J. Fedro, Phys. Rev. B **45**, 7588 (1992).
- 36 S.-L. Drechsler, J. Malek, S. Zalis, and K. Rościszewski, Phys. Rev. B, **53**, 11 328 (1996); J. of Superconductivity **9**, 439 (1996); *ibid.* **10** in press.
- 37 Strictly speaking, the fit of the dispersion along the **a**-direction requires more Fourier-components. However, their individual weight is small with respect to the interchain exchange. It can be expected that within a proper treatment of the local electron correlation the influence of far reaching hopping integrals should be reduced.
- 38 W. Geertsma and D. Khomskii, Phys. Rev. B **54**, 3011 (1996); D. Khomskii, W. Geertsma, and M. Mostovoy, Proc. LT21 Prague 1996, Czech Journal of Physics, **46**-Suppl. part 6, 3239 (1996).
- 39 K. Schulten, I. Ohmine, and M. Karplus, J. of Chem. Phys. **64**, 4442 (1976).
- 40 A. Ovchinnikov, Zh. Eksp. Teor. Fiz. **57**, 2137 (1969) (or Sov. Phys. JETP **30**, 1160 (1970)).
- 41 K. Okada, A. Kotani, K. Maiti, and D.D. Sarma, J. Jpn. **56**, 1844 (1996)
- 42 K. Maiti, D.D. Sarma, T. Mizokawa, and A. Fujimori, Europhysics Lett. **37**, 359 (1997).
- 43 I. Terasaki, R. Itti, N. Koshizuka, M. Hase, I. Tsukuda, and K. Uchinokura, Phys. Rev. B, **52**, 295 (1995).
- 44 D. Gottlieb, M. Lagos, K. Hallberg, and C. Balseiro, Phys. Rev. B **43**, 13 668 (1991).
- 45 A. Fledderjohann and C. Gros, *sisso-preprint cond-mat/9612013* (1996).
- 46 W. Stephan and K. Penc, Phys. Rev. B **54**, R 17 269 (1996).
- 47 H. Suzuura, H. Yasuhara, A. Furusaki, N. Nagaosa, and Y. Tokura, Phys. Rev. Lett. **76**, 2579 (1996).
- 48 J. Lorenzana and R. Eder, Phys. Rev. B **55**, R3358 (1997).
- 49 R. Neudert *et al.* to be published.
- 50 The attribution of sharp peaks near 1.25 eV, 2.9 eV and 3.66 eV observed in $\text{Im}\varepsilon(\omega)$ to the *dp* charge transfer gap which is of interest here, to *dd*-transitions, and to Ge-states related interband transition is controversé.
- 51 T. Osafune, N. Motoyama, H. Eisaki, and S. Uchida, Phys. Rev. Lett. **78**, 1980 (1997).

- ⁵² Y. Mizuno, T. Tohyama, and S. Maekawa, J. Phys. Soc. Jap. to be published; sissa-preprint cond-mat/9612252 (1996).
- ⁵³ L. Feiner, J. Jefferson, and R. Raimondi, Phys. Rev. B **53**, 8751 (1996).
- ⁵⁴ S.-L. Drechsler, J. Malek, and H. Eschrig, Phys. Rev. B **55**, 606 (1997).
- ⁵⁵ M. Nishi, O. Fujita, J. Akimitsu, K. Kakurai, and Y. Fujii, Physica **B** 213 & 214, 275 (1995).
- ⁵⁶ N. Majilis, S. Selzer, and G. Strinati, Phys. Rev. B **45**, 7872 (1992).
- ⁵⁷ H. Fukuyama, T. Tanimoto, and M. Saito, J. of Phys. Soc. Jap. **65**, 1182 (1996).
- ⁵⁸ M. Honda, T. Shirata, K. Kindo, S. Sugai, T. Takeuchi, and H. Hori, J. of Phys. Soc. Jap. **65**, 691 (1996).
- ⁵⁹ H. Schulz in “Low Dimensional Conductors and Superconductors” (Eds. D. Jerome and L.G. Caron), NATO ASI series **155**, p. 95, Plenum Press, New York (1987).

TABLES

TAB. Model parameters for Sr_2CuO_3 , Ca_2CuO_3 and CuGeO_3 . The LDA-LCAO derived tight binding parameters in the first group of rows are explained in Sec. II. The LDA-numbers for CuGeO_3 are estimated from Figs. 2 of Ref. [24] and Ref. [25]. The second group contains experimental values (in the case of several data we prefer the underlined) which were used in addition to the band-structure information to estimate the corresponding parameters of the extended Hubbard model as well as the exchange integrals of the anisotropic Heisenberg-model (third group of rows). They are derived and discussed in Sec. III. The experimental magnetic moment μ^{exp} (given together with T_N in group IV) may be compared with μ^{CSC} derived from Eq. (19) using the experimental data for the in-chain exchange integrals J_{\parallel} and our estimation of J_{\perp} . Vice versa, the experimental μ^{exp} determines via the same Eq. (19) the empirical inter-chain exchange integrals J_{\perp}^{emp} .

group	quantity	Sr ₂ CuO ₃	Ca ₂ CuO ₃	CuGeO ₃ (GeCu _{1-x} Zn _x O ₃)
I	$t_{1,LDA}/\text{meV}$	550	520	250
	$t_{2,LDA}/\text{meV}$	100	100	81
	t_{\perp}/meV	20 to 30	50 to 65	25 to 33
II	E_g/eV	(1.8 to 1.9) ^{a,b}	(2.1) ^c	(1.25) ^d , (3.7) ^e
	J/meV (= J_{\parallel}/meV)	(140) ^f , (190) ^g , (260) ^h	(160) ⁱ (254) ^h	(11 ± 1) ^j , (22) ^k
III	t_1/meV	410	419	187
	t_2/meV	100	100	90
	U_{eff}/eV	(3.15) ^b	3.5	4.34 (4.2) ^e
	V_1/eV	0.21	0.16	0.1
	$ K /\text{meV}$	11	30	19
	J_{\perp}/meV	0.5 to 1.1	2.9 to 4.3	0.6 to 1, (1.1) ^l
IV	T_N/K	(5) ^l	(8...10) ^l	(4.5) ^m
	μ^{exp}/μ_B	(0.06±0.01) ^l	(0.09±0.01) ^l	(0.23) ^j
V	μ^{CSC}/μ_B	0.08 to 0.11	0.19 to 0.24	0.35 to 0.45
	$J_{\perp}^{emp}/\text{meV}$	0.3± 0.1	0.6±0.1	0.27

^a Raman resonance, Ref. [11]

^b EELS, Ref. [49]

^c opt. absorption, Ref. [5]

^d XPS, Ref. [43]

^e XPS, Ref. [30]

^f magn. suscept., Ref. [8,9]

^g magn. suscept., Refs. [10]

^h midinfrared, Ref. [47]

ⁱ theory, Ref. [36]

^j INS, Raman, Refs. [27,29,31,45]

^k Raman, Ref. [28]

^l μ SR, Ref. [15]

^m INS, Ref. [55]

FIGURES

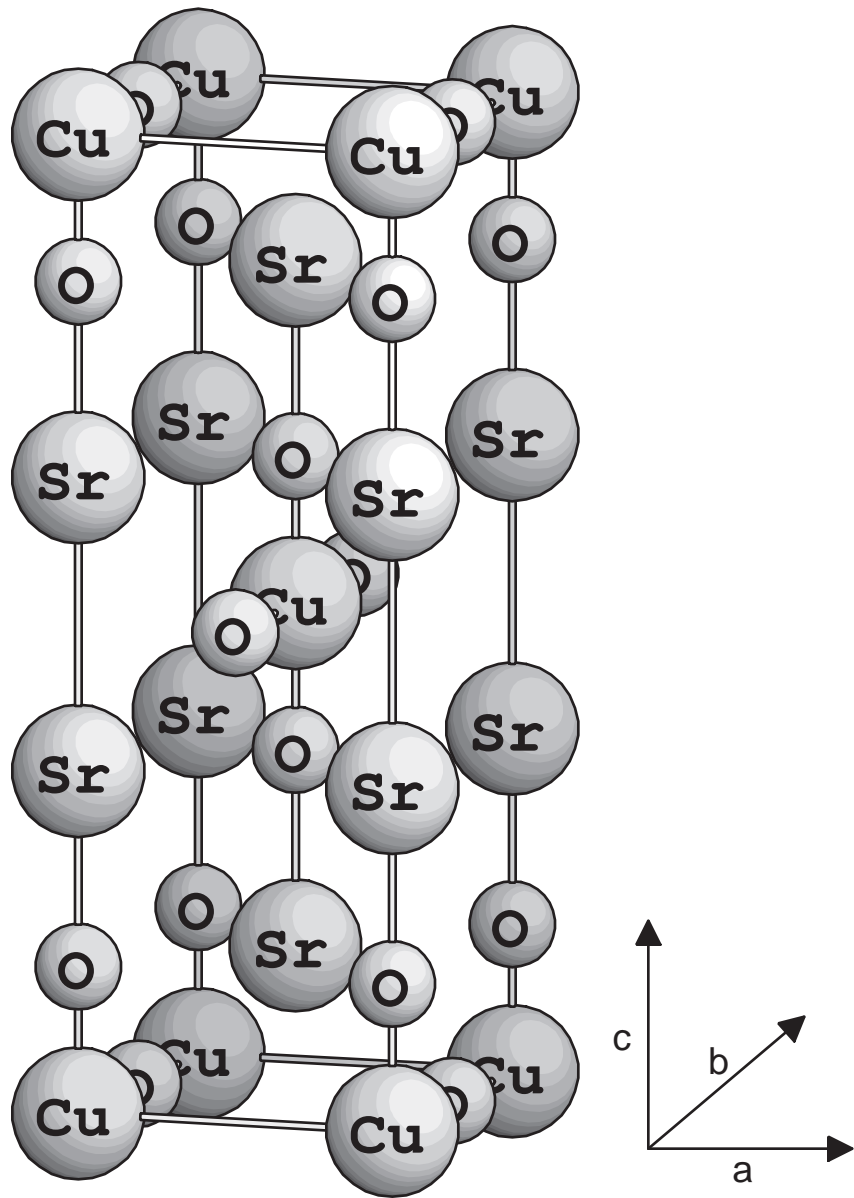
FIG. 1 Crystal structure of Sr_2CuO_3

FIG. 2 LCAO energy-bands near the Fermi level for Sr_2CuO_3 along high-symmetry Brillouin-zone directions within the (k_x, k_y) plane. The momenta are given in units of $(\pi/a, \pi/b)$. Strong dispersion can be seen along $(0,0)$ – $(0,1)$ (**b**-direction, parallel to the CuO_3 chains) whereas a small, but non-negligible dispersion in the perpendicular **a**-direction can be seen.

FIG. 3 Density of states $N(E)$ for Sr_2CuO_3 . The insert shows the partial Cu $3d$ and $4s$ density of states of the nearly one-dimensional band crossing the Fermi level.

FIG. 4 Dispersion of the nearly one-dimensional band. The insert is for fixed $k_y = k_{y\text{Fermi}} = \pi/2b$.

FIG. 5 Dependence of the transfer integral t_1 (upper panel) and the on-site Coulomb interaction U_{eff} (lower panel) of the Hubbard model according to its Bethe ansatz-solution *vs.* inchain superexchange integral J_1^{AF} (lower panel) in the strong coupling limit for typical values of the optical gap E_g . The experimental values for J_1^{AF} are depicted by arrows. They are determined from the total exchange integral J adopting ferromagnetic and second neighbor contributions discussed in the text.



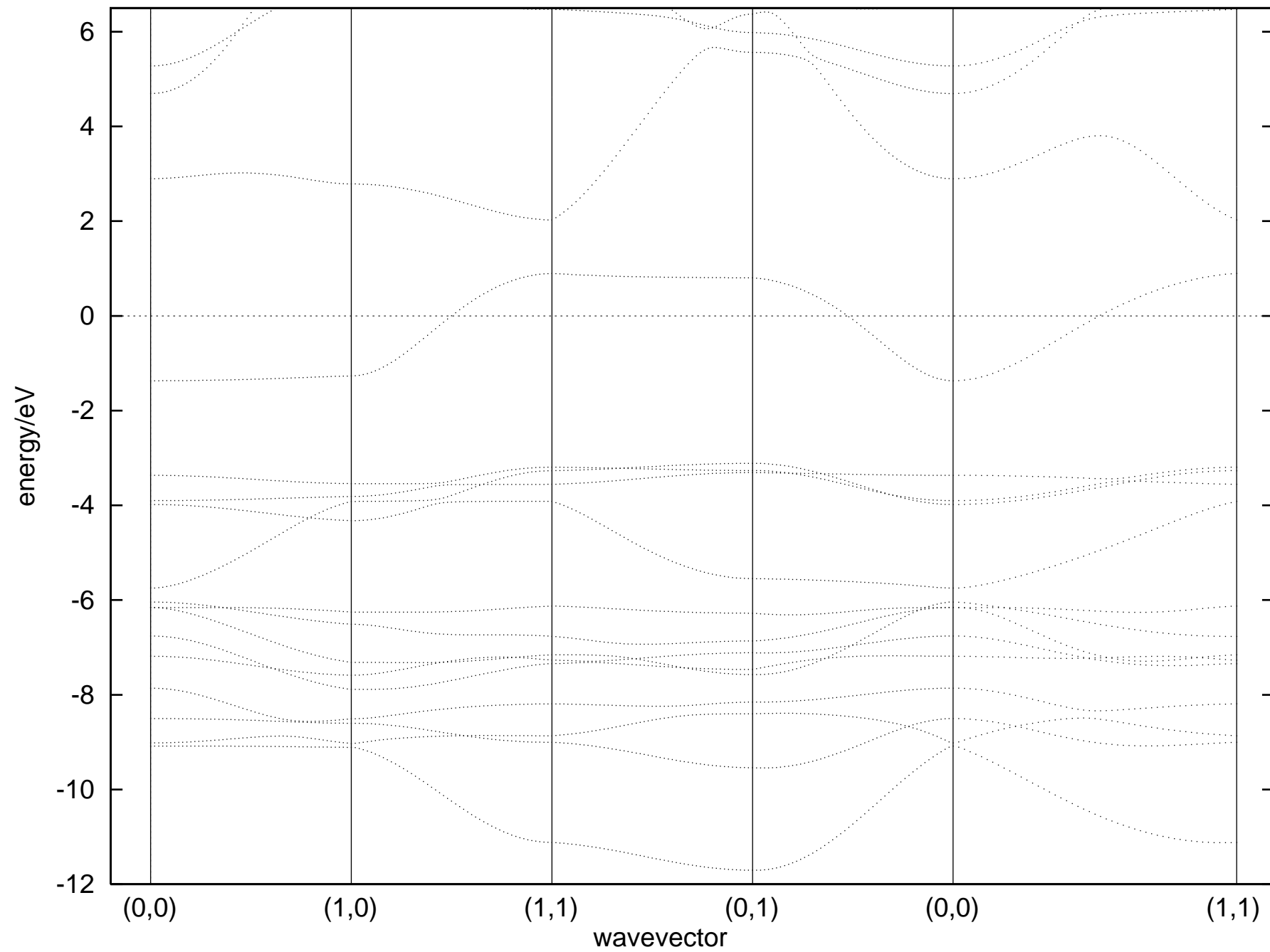


Fig. 2 Rosner et.al.

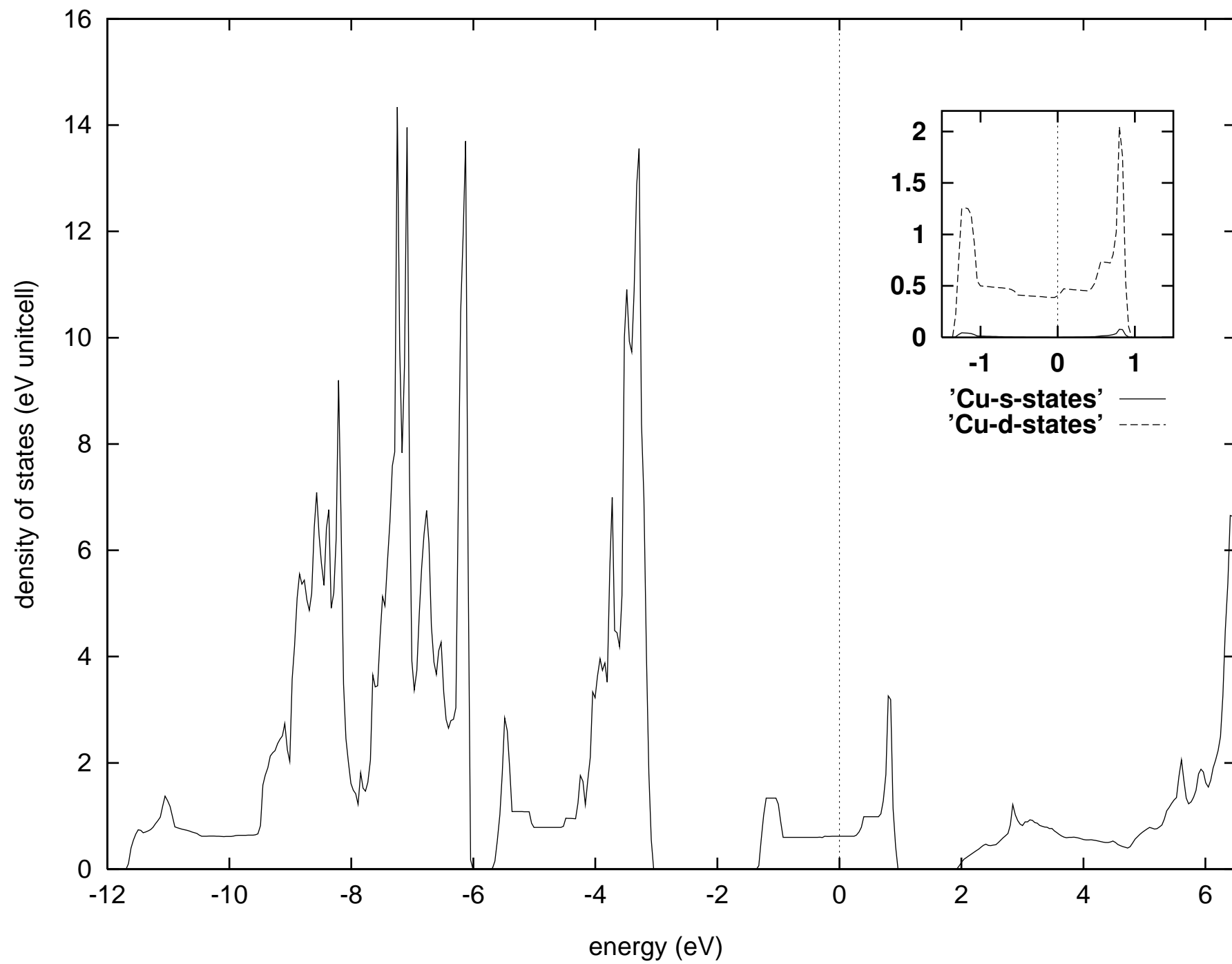


Fig. 3 Rosner et al.

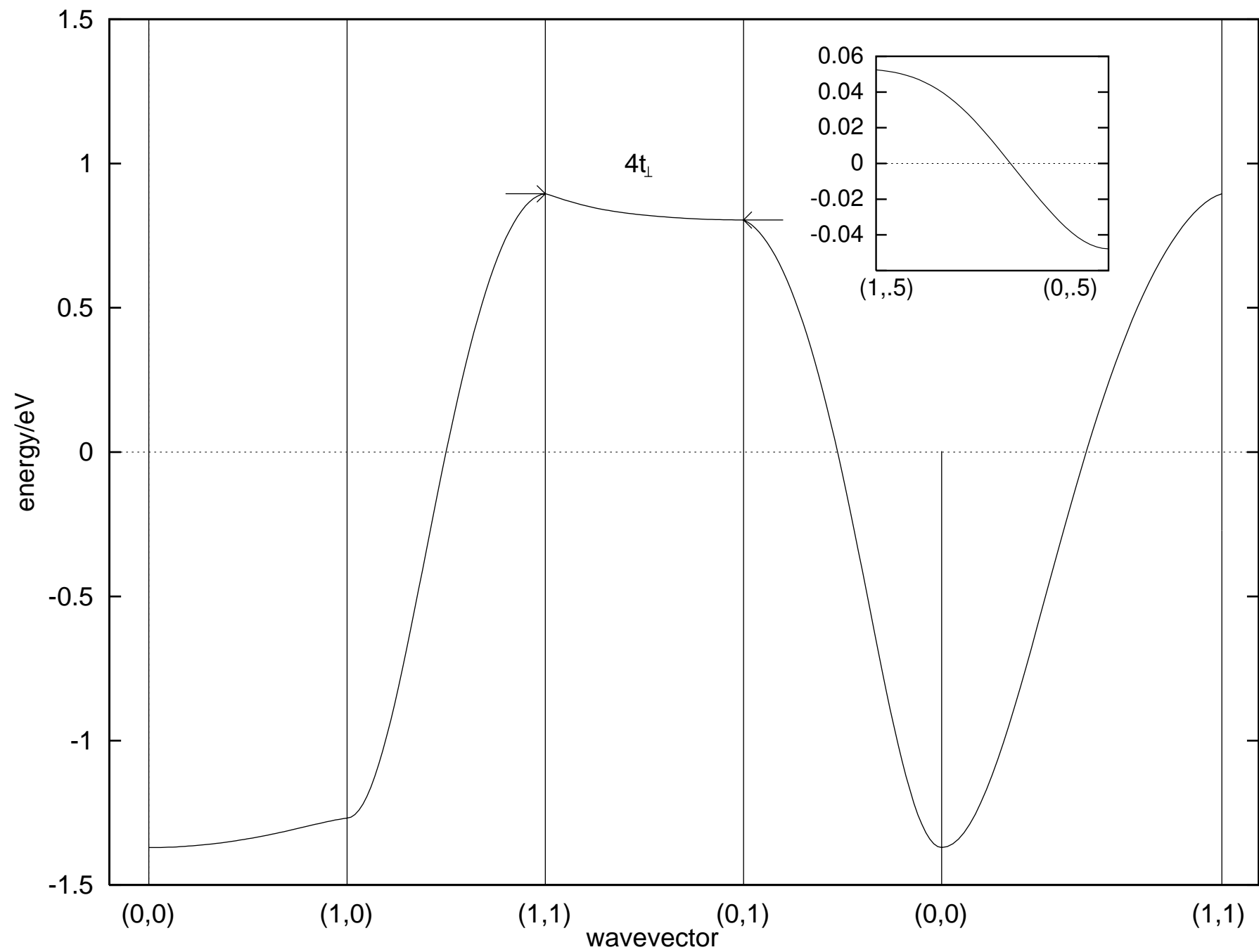


Fig. 4 Rosner et.al.

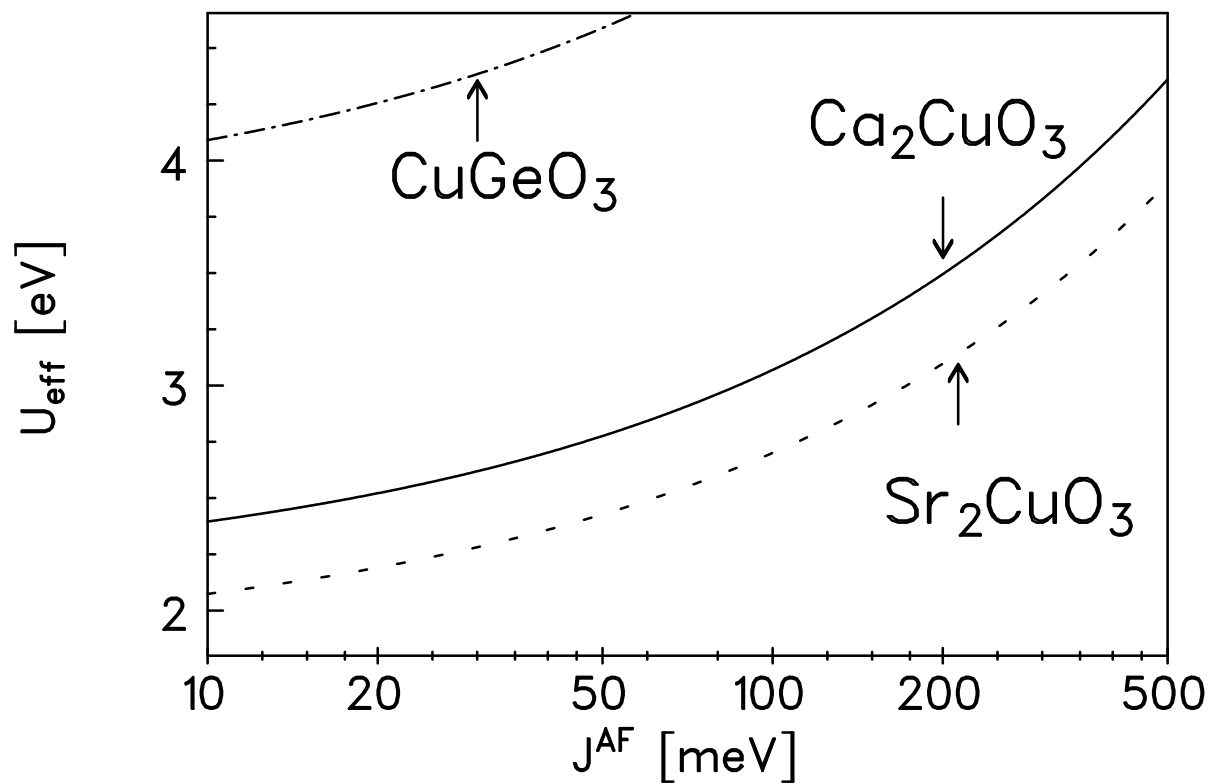
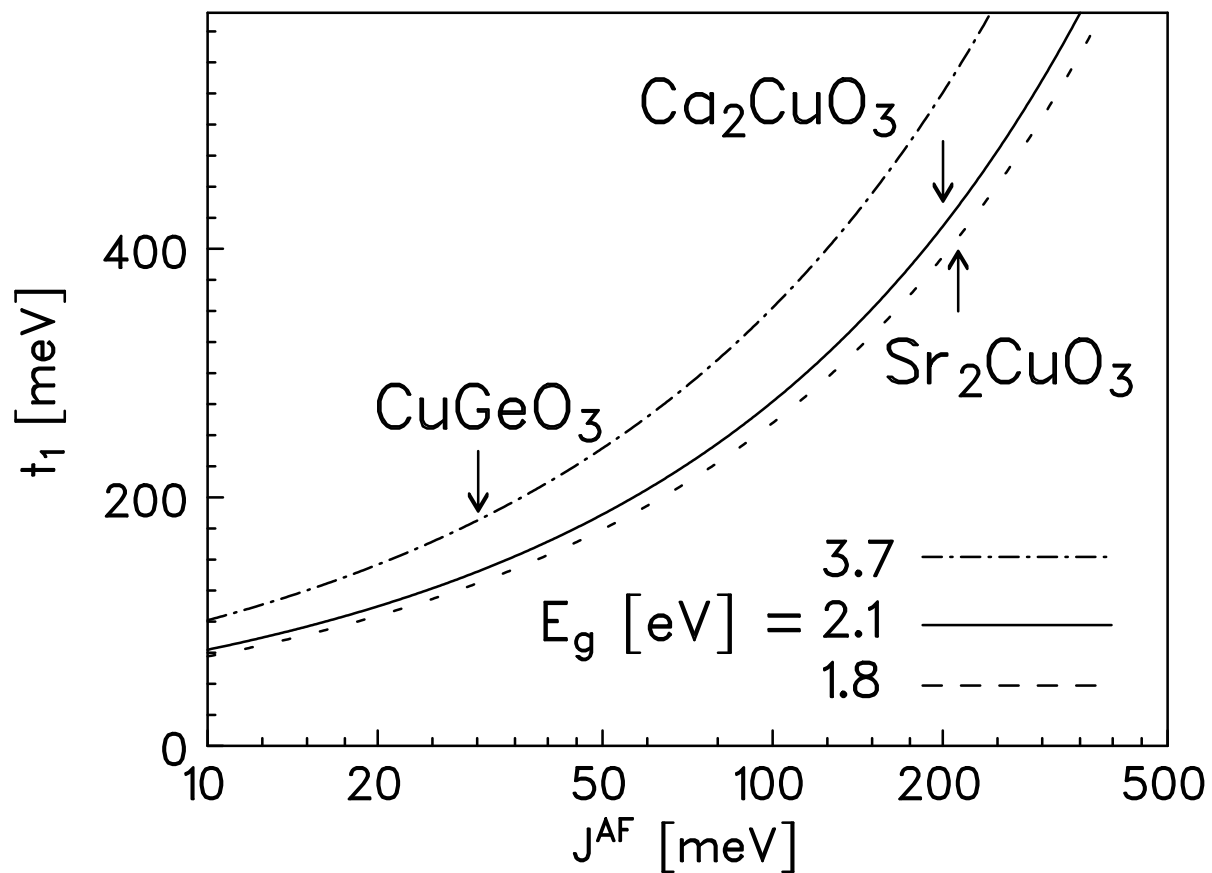


Fig. 5
 Rosner et al.